Potential energy surfaces for cluster emitting nuclei

Dorin N. Poenaru,[1,2,*] Radu A. Gherghescu,[1,2] and Walter Greiner[2]

[1] *Horia Hulubei National Institute of Physics and Nuclear Engineering, RO-077125 Bucharest-Magurele, Romania*

[2] *Frankfurt Institute for Advanced Studies, J. W. Goethe Universität, Max-von-Laue-Str. 1, D-60438 Frankfurt am Main, Germany*

(Dated: September 27, 2005)

Potential energy surfaces are calculated by using the most advanced asymmetric two-center shell model allowing to obtain shell and pairing corrections which are added to the Yukawa-plus-exponential model deformation energy. Shell effects are of crucial importance for experimental observation of spontaneous disintegration by heavy ion emission. Results for ^{222}Ra, ^{232}U, ^{236}Pu and ^{242}Cm illustrate the main ideas and show for the first time for a cluster emitter a potential barrier obtained by using the macroscopic-microscopic method.

PACS numbers: 24.75.+i, 25.85.Ca, 27.90.+b

INTRODUCTION

Recently we performed a systematic analysis [1] of the experimental results concerning heavy particle radioactivities [2] showing that our predictions within the analytical superasymmetric (ASAF) model (see [3] and the references therein) have been confirmed and that the strong shell effects of the daughter ^{208}Pb were not fully exploited. In this way we could make suggestions for the candidates to be used in the future experiments.

In the present work we take advantage of using the most advanced two center shell model [4] to study the potential energy surfaces (PES) of cluster emitting nuclei showing deep valleys due to the doubly magic heavy fragments ^{208}Pb and ^{132}Sn. The Strutinsky's [5] macroscopic-microscopic method is used. A particularly deep valley is that of ^{208}Pb which proved to be of practical importance not only for the production of superheavy nuclei but also for experimental search of cluster decay modes. Even for alpha decay it is possible to see such a valley if the emitter is ^{212}Po or ^{106}Te. In the later case the heavy fragment ^{102}Sn plays the important role. The potential barrier shape for a heavy ion decay mode may be obtained by cutting the PES at a given value of the mass and charge asymmetry. In this way one can compare the difference between the macroscopic barrier and the total one with shell and pairing corrections taken into account, providing a further justification of the ASAF barrier shape.

MACROSCOPIC ENERGY

In a binary fission process $^{A}Z \rightarrow {}^{A_1}Z_1 + {}^{A_2}Z_2$ the phenomenological energy E_{Y+EM} is calculated within Yukawa-plus-exponential model (Y+EM) [6, 7] by taking into account the difference between charge and mass asymmetry [8].

By requesting zero deformation energy for a spherical shape, the potential energy is defined as

$$\begin{aligned} E_{Y+EM} &= (E_Y - E_Y^0) + (E_c - E_c^0) \\ &= E_Y^0[B_Y - 1 + 2X(B_c - 1)] \end{aligned} \quad (1)$$

where $E_Y^0 = a_2 A^{2/3}\{1 - 3x^2 + (1 + 1/x)[2 + 3x(1 + x)]\exp(-2/x)\}$, $E_c^0 = a_c Z^2 A^{-1/3}$ are energies corresponding to spherical shape and $a_2 = a_s(1 - \kappa I^2)$, $I = (N - Z)/A$, $x = a/R_0$, $R_0 = r_0 A^{1/3}$. The parameters $a_s, \kappa, a_c = 3e^2/(5r_0)$, and r_0 are taken from Möller et al. [9].

The relative Yukawa and Coulomb energies $B_Y = E_Y/E_Y^0$, $B_c = E_c/E_c^0$ are functions of the nuclear shape. The dependence on the neutron and proton numbers is contained in E_Y^0, in the fissility parameter $X = E_c^0/(2E_Y^0)$ and B_Y. For a binary fragmentation with charge densities ρ_{1e} and ρ_{2e}, one has [8] a relative energy

$$B_Y = \frac{E_Y}{E_Y^0} = \frac{a_{21}}{a_{20}}B_{Y1} + \frac{\sqrt{a_{21}a_{22}}}{a_{20}}B_{Y12} + \frac{a_{22}}{a_{20}}B_{Y2} \quad (2)$$

with axially-symmetric shape-dependent terms expressed by triple integrals

$$B_{Y1} = b_Y \int_{-1}^{x_c} dx \int_{-1}^{x_c} dx' \int_0^1 dw F_1 F_2 Q_Y \quad (3)$$

$$B_{Y12} = b_Y \int_{-1}^{x_c} dx \int_{x_c}^{1} dx' \int_0^1 dw F_1 F_2 Q_Y \quad (4)$$

$$B_{Y2} = b_Y \int_{x_c}^{1} dx \int_{x_c}^{1} dx' \int_0^1 dw F_1 F_2 Q_Y \quad (5)$$

in which $b_Y = -d^4(r_0/2a^2)a_2 R_0 A/E_Y^0$, $d = (z'' - z')/2R_0$ is the nuclear semilength in units of R_0 and

$$F_1 = y^2 + yy_1\cos\varphi - \frac{x - x'}{2}\frac{dy^2}{dx} \quad (6)$$

$$Q_Y = \{[\sqrt{P}(\sqrt{P}+2a/R_0d)+2a^2/(R_0d)^2]\cdot \exp(-R_0\sqrt{P}d/a)-2a^2/(R_0d)^2\}/P^2 \quad (7)$$

F_2 is obtained from F_1 by replacing dy^2/dx with dy_1^2/dx'. In the above equations $P=y^2+y_1^2-2yy_1\cos\varphi+(x-x')^2$, $w=\varphi/2\pi$, and x_c is the position of separation plane between fragments with -1, +1 intercepts on the symmetry axis (surface equation $y=y(x)$ or $y_1=y(x')$). The integrals are computed numerically by Gauss-Legendre quadratures.

In a similar way the Coulomb relative energy is given by

$$B_c=\frac{E_c}{E_c^0}=\left(\frac{\rho_{1e}}{\rho_{0e}}\right)^2 B_{c1}+\frac{\rho_{1e}\rho_{2e}}{\rho_{0e}^2}B_{c12}+\left(\frac{\rho_{2e}}{\rho_{0e}}\right)^2 B_{c2} \quad (8)$$

and for axially symmetric shapes

$$B_{c1}=b_c\int_{-1}^{x_c}dx\int_{-1}^{x_c}dx'F(x,x') \quad (9)$$

$$B_{c12}=b_c\int_{-1}^{x_c}dx\int_{x_c}^{1}dx'F(x,x') \quad (10)$$

$$B_{c2}=b_c\int_{x_c}^{1}dx\int_{x_c}^{1}dx'F(x,x') \quad (11)$$

where $b_c=5d^5/8\pi$. In the integrand

$$F(x,x')=\{yy_1[(K-2D)/3]\cdot \left[2(y^2+y_1^2)-(x-x')^2+\tfrac{3}{2}(x-x')\left(\tfrac{dy_1^2}{dx'}-\tfrac{dy^2}{dx}\right)\right]+K\left\{y^2y_1^2/3+\left[y^2-\tfrac{x-x'}{2}\tfrac{dy^2}{dx}\right]\cdot\left[y_1^2-\tfrac{x-x'}{2}\tfrac{dy_1^2}{dx'}\right]\right\}\}a_\rho^{-1} \quad (12)$$

K and K' are the complete elliptic integrals of the first and second kind, respectively:

$$K(k)=\int_0^{\pi/2}(1-k^2\sin^2t)^{-1/2}dt \quad (13)$$

$$K'(k)=\int_0^{\pi/2}(1-k^2\sin^2t)^{1/2}dt \quad (14)$$

and $a_\rho^2=(y+y_1)^2+(x-x')^2$, $k^2=4yy_1/a_\rho^2$, $D=(K-K')/k^2$. The elliptic integrals may be calculated by using Chebyshev polynomial approximation. For $x=x'$ the function F is not determined. In this case, after removing the indetermination, we get $F(x,x')=4y^3/3$.

Starting from the touching point configuration, $R\geq R_t$, for spherical shapes of the fragments, one can use *analytical relationships.* The Coulomb interaction energy of a system of two spherical nuclei, separated by a distance R between centers, is $E_{c12}=e^2Z_1Z_2/R$, where e is the electron charge.

Within a liquid drop model (LDM) there is no contribution of the surface energy to the interaction of the separated fragments; the barrier has a maximum at the touching point configuration. The proximity forces acting at small separation distances (within the range of strong interactions) give rise in the Y+EM to an interaction term expressed as folllows

$$E_{Y12}=-4\left(\frac{a}{r_0}\right)^2\sqrt{a_{21}a_{22}}\frac{\exp(-R/a)}{R/a}\cdot\left[g_1g_2\left(4+\frac{R}{a}\right)-g_2f_1-g_1f_2\right] \quad (15)$$

where

$$g_k=\frac{R_k}{a}\cosh\left(\frac{R_k}{a}\right)-\sinh\left(\frac{R_k}{a}\right) \quad (16)$$

$$f_k=\left(\frac{R_k}{a}\right)^2\sinh\left(\frac{R_k}{a}\right) \quad (17)$$

In many cases the interaction energy is maximum at a certain distance $R_m>R_t=R_1+R_2$, which can be found by solving numerically the following nonlinear equation

$$e^x+p_1+x(p_1+xp)=0\ ;\ x=R/a \quad (18)$$

in which

$$p=-\frac{a^3}{r_0^2}\sqrt{a_{21}a_{22}}\frac{g_1g_2}{e^2Z_1Z_2} \quad (19)$$

$$p_1=p(4-f_1/g_1-f_2/g_2) \quad (20)$$

and the interval $x_t=R_t/a, x_t+5$ may be given as input data of a program using Müller's iteration scheme of succesive bisections and inverse parabolic interpolation.

SHELL AND PAIRING CORRECTIONS

In the following we would like to outline the calculations of the shell [5] and pairing [10] corrections $\delta E=\delta U+\delta P$ leading to the total deformation energy

$$E_{def}(R,\eta)=E_{Y+EM}(R,\eta)+\delta E(R,\eta) \quad (21)$$

More details are given in the book [2]. By choosing two intersected spheres for nuclear shape parametrization one can take the separation distance between fragment centers, R, as a deformation parameter. Initially, for a parent nucleus $R_i=R_0-R_2$. At the touching point $R_t=R_1+R_2$. The mass asymmetry $\eta=(A_1-A_2)/A$.

The two-center shell model [4] gives at every pair of coordinates (R,η) the sequence of doubly degenerate

discrete energy levels $\epsilon_i = E_i/\hbar\omega_0^0$ in units of $\hbar\omega_0^0 = 41A^{-1/3}$, arranged in order of increasing energy. The smoothed-level distribution density is obtained by averaging the actual distribution over a finite energy interval $\Gamma = \gamma\hbar\omega_0^0$, with $\gamma \simeq 1$,

$$\tilde{g}(\epsilon) = \{\sum_{i=1}^{n_m}[2.1875 + y_i(y_i(1.75 - y_i/6) - 4.375)]e^{-y_i}\}\,(1.77245385\gamma)^{-1} \quad (22)$$

where $y = x^2 = [(\epsilon - \epsilon_i)/\gamma]^2$. The summation is performed up to the level n_m fulfilling the condition $|x_i| \geq 3$.

The Fermi energy, $\tilde{\lambda}$, of this distribution is given by

$$N_p = 2\int_{-\infty}^{\tilde{\lambda}} \tilde{g}(\epsilon)d\epsilon \quad (23)$$

with $N_p = Z$ for proton levels and $N_p = A - Z$ for neutron levels, leading to a non-linear equation in $\tilde{\lambda}$, solved numerically. The total energy of the uniform level distribution

$$\tilde{u} = \tilde{U}/\hbar\omega_0^0 = 2\int_{-\infty}^{\tilde{\lambda}} \tilde{g}(\epsilon)\epsilon d\epsilon \quad (24)$$

In units of $\hbar\omega_0^0$ the shell corrections are calculated for each pair (R, η):

$$\delta u(n, R, \eta) = \sum_{i=1}^{n} 2\epsilon_i(R, \eta) - \tilde{u}(n, R, \eta) \quad (25)$$

$n = N_p/2$ particles. Then $\delta u = \delta u_p + \delta u_n$.

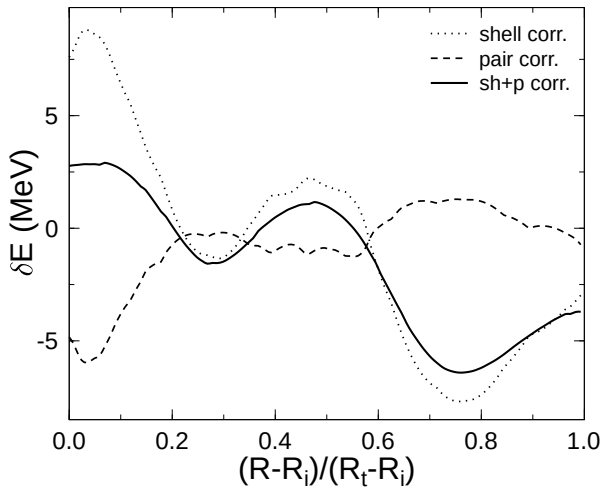

FIG. 1: Shell and pairing corrections for a symmetric ($\eta = 0$) fission of ^{236}Pu.

Similarly, for pairing corrections we take the doubly degenerate levels $\{\epsilon_i\}$ in units of $\hbar\omega_0^0$. $Z/2$ levels are occupied with n levels below and n' above Fermi energy contributing to pairing, $n = n' = \Omega\tilde{g}_s/2$. The cutoff energy, $\Omega \simeq 1 \gg \tilde{\Delta} = 12/\sqrt{A}\hbar\omega_0^0$. The gap Δ and Fermi energy λ are solutions of the BCS system of two eqs:

$$0 = \sum_{k_i}^{k_f} \frac{\epsilon_k - \lambda}{\sqrt{(\epsilon_k - \lambda)^2 + \Delta^2}} \quad (26)$$

$$\frac{2}{G} = \sum_{k_i}^{k_f} \frac{1}{\sqrt{(\epsilon_k - \lambda)^2 + \Delta^2}} \quad (27)$$

where $k_i = Z/2 - n + 1$, $k_f = Z/2 + n'$, and

$$\frac{2}{G} \simeq 2\tilde{g}(\tilde{\lambda})\ln\left(\frac{2\Omega}{\tilde{\Delta}}\right) \quad (28)$$

As a consequence of the pairing correlation, the levels below the Fermi energy are only partially filled, while those above the Fermi energy are partially empty. Occupation probability by a quasiparticle (u_k) or hole (v_k) is given by

$$v_k^2 = [1 - (\epsilon_k - \lambda)/E_k]/2; \;\; u_k^2 = 1 - v_k^2 \quad (29)$$

The quasiparticle energy is expressed as

$$E_\nu = \sqrt{(\epsilon_\nu - \lambda)^2 + \Delta^2}. \quad (30)$$

The pairing correction $\delta p = p - \tilde{p}$, represents the difference between the pairing correlation energies for the discrete level distribution

$$p = \sum_{k=k_i}^{k_f} 2v_k^2\epsilon_k - 2\sum_{k=k_i}^{Z/2} \epsilon_k - \frac{\Delta^2}{G} \quad (31)$$

and for the continuous level distribution

$$\tilde{p} = -(\tilde{g}\tilde{\Delta}^2)/2 = -(\tilde{g}_s\tilde{\Delta}^2)/4 \quad (32)$$

Compared to shell correction, the pairing correction is out of phase and smaller (see Fig.1) leading for $\eta =$ constant to a smoother total curve $\delta e(R) = \delta u(R) + \delta p(R)$ where $\delta p = \delta p_p + \delta p_n$.

RESULTS

In the following we shall present results for ^{222}Ra, ^{232}U, ^{236}Pu, and ^{242}Cm, which are emitters of ^{14}C, ^{24}Ne, ^{28}Mg, and ^{34}Si, respectively. All have been experimentally observed. In order to obtain a relatively smooth PES we made the approximation $\eta = \eta_A = (A_1 - A_2)/A \simeq \eta_Z = (Z_1 - Z_2)/Z$. In this way the fragment nucleon numbers N_1, Z_1 and N_2, Z_2 (plotted in figures 6, 11, 16, 21) are linear functions of η. We prefer to use the dimensionless separation distance $\xi = (R - R_i)/(R_t - R_i)$ instead of R. In this way one can clearly see the initial parent nucleus at $\xi = 0$ and the touching point configuration at $\xi = 1$. We adopt the usual convention of having zero deformation energy and shell plus pairing corrections for the initial spherical shape, leading to $E_{def} = E_{Y+EM} = \delta E = 0$ at $R = R_i$ for all values of η and at $\eta = \pm 1$ for all values of R.

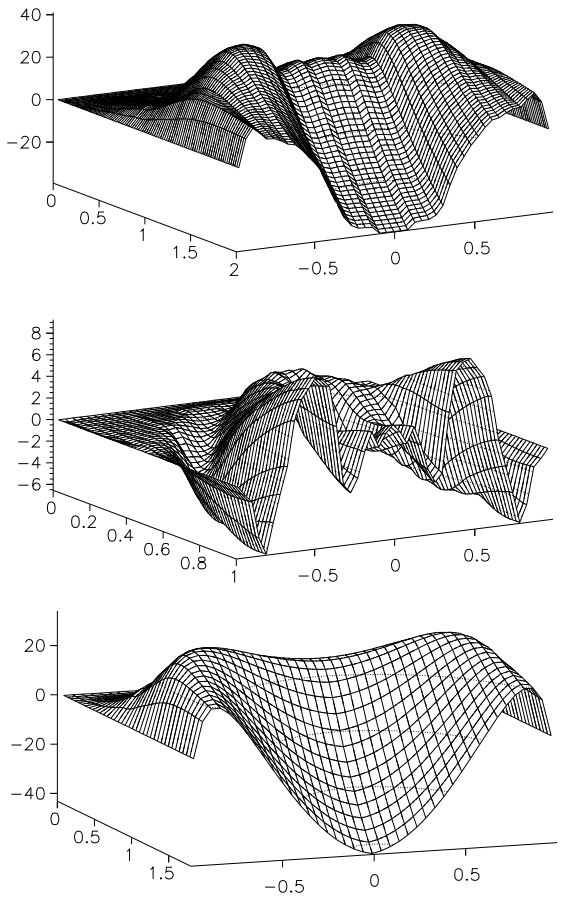

FIG. 2: PES of ^{222}Ra vs $(R-R_i)/(R_t-R_i) \geq 0$ and $\eta = (A_1 - A_2)/(A_1 + A_2)$. Y+EM (bottom), Shell + Pairing corrections (center), and total deformation energy (top). The energies are expressed in MeV.

^{222}Ra

The PES versus the normalized separation distance $(R - R_i)/(R_t - R_i)$ and the mass asymmetry $\eta = (A_1 - A_2)/(A_1 + A_2)$ are plotted in Fig. 2. The macroscopic Y+EM deformation energy is shown at the bottom, followed by the microscopic shell plus pairing corrections (center), and their sum (the total deformation energy) at the top.

Three valleys around $\eta \simeq 0.8$; 0.3 and 0.1 can be seen in the center of Fig. 2 and on the corresponding contour plot (Fig. 3). We only count the number of valleys for $\eta \geq 0$ because the mirror $\eta \leq 0$ gives the same number for complimentary heavy fragments becoming light ones and vice-versa. In figure 6 we shall see that they are produced due to the magicity of the nucleon number of the fragments. Such cold valleys were used in the sixtieth by Walter Greiner to motivate the search for superheavy elements, and the development of Heavy Ion Physics worldwide and in Germany, where GSI was built. These valleys may be also seen on the total PES at the top of Fig. 2. Here the deepest valley remains that at a small value of η not far from the minimum of the macroscopic Y+EM energy at $\eta = 0$, which is responsible for the cold fission. At a large value of η, the ^{208}Pb + ^{14}C

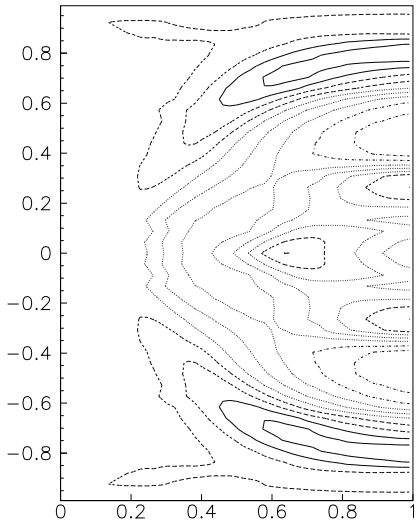

FIG. 3: Contour plot of shell and pairing corrections for ^{222}Ra vs $(R - R_i)/(R_t - R_i)$ and η.

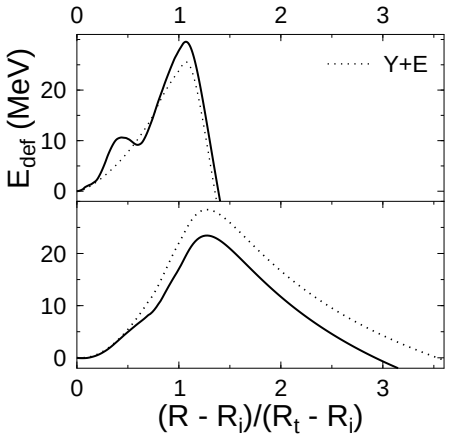

FIG. 4: A cut through the PES of ^{222}Ra at symmetry $\eta = 0$ (top) and for ^{14}C radioactivity with ^{208}Pb daughter (bottom).

valley, favouring the ^{14}C radioactivity of ^{222}Ra, is laying on the Businaro-Gallone mountain, hence it is shallower despite the fact that it is very pronounced in the shell correction surface. On the contour plot (figure 3) one can see how it evolves from lower mass asymmetry at a

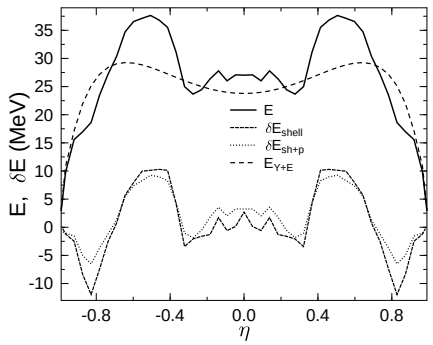

FIG. 5: Deformation energies at the touching point configurations ($R = R_t$) of ^{222}Ra vs the asymmetry η: E_{Y+EM} and E_{def} (top); shell + pairing corrections and only shell corrections (bottom).

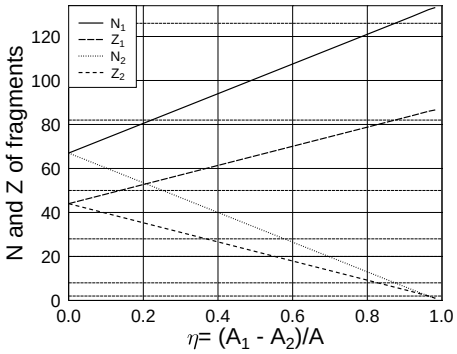

FIG. 6: Variation of the neutron and proton numbers of the two fragments with the mass asymmetry at the touching point, $R = R_t$ for ^{222}Ra.

small value of separation distance, ξ, to the larger η at the touching point, $\xi = 1$.

Two plots obtained by cutting the total PES and that of Y+EM at a given value of the asymmetry parameter are shown in Fig. 4. In the upper part one can see a two humped barrier at $\eta = 0$. The typical example for ^{14}C emission from ^{222}Ra, shown at the bottom, provide justification for one of the basic assumption of the analytical superasymmetric fission model, which was very successful in predicting the half-lives of cluster decay modes. It is remarkable to see for the first time for a cluster emitter a potential barrier obtained by using the macroscopic-microscopic method. Having a smaller height and width compared to the (dotted line) macroscopic Y+EM barrier, it is very similar to the barrier used in ASAF which was lower and narrower than the Myers-Swiatecki's [11] LDM barrier.

One can see how deep are the two main valleys on the PES by plotting in Fig. 5 a cut of the PES at the touching point configuration, $R = R_t$. In the upper part of this figure the macroscopic energy, E_{Y+E} (the smooth dashed line), and the total deformation energy, E (heavy line) can be seen. In the lower part of Fig. 5 there are two other curves representing the shell plus pairing correction (dotted curve) and only the shell corrections (dashed line). As we already mentioned when the Fig. 1 was discussed, there are two effects of pairing corrections leading to a smoother variation and to a shallower valley.

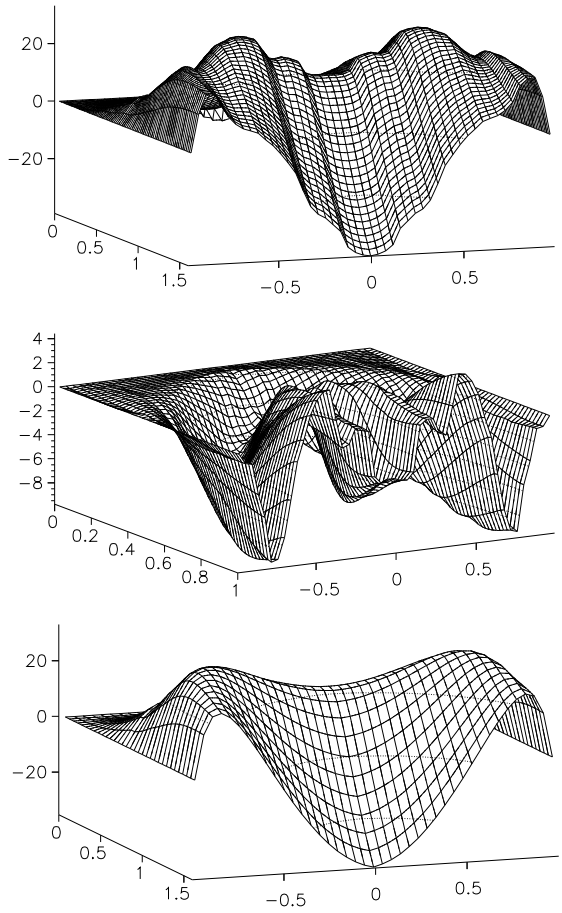

FIG. 7: PES of ^{232}U vs $(R - R_i)/(R_t - R_i)$ and $\eta = (A_1 - A_2)/(A_1 + A_2)$. Y+EM (bottom), Shell + Pairing corrections (center), and total deformation energy (top). The energies are expressed in MeV.

We can better understand how the deep valleys appear in figure 5 if we plot in figure 6 the variation of the neutron and proton numbers of the two fragments with the mass asymmetry at the touching point, $R = R_t$, for ^{222}Ra. Every time a nucleon number reaches a magic value, the corresponding shell correction has a local minimum. The very deep valley at $\eta > 0.8$ (for different mass and charge asymmetry at $\eta_A = 0.874$ and $\eta_Z = 0.864$) is produced by reaching almost simultaneously three magic numbers $N_1 = 126$, $N_2 = 8$, and $Z_1 = 82$ (the decay $^{222}\text{Ra} \rightarrow {}^{208}\text{Pb} + {}^{14}\text{C}$). The next one, at an intermediate value of η ($\eta_A = 0.369$, $\eta_Z = 0.363$), is mainly due

to the Ni ($Z_2 = 28$) light fragment (^{222}Ra $\rightarrow$ ^{152}Nd + $^{70}_{28}$Ni$_{42}$). Finally the valley at a small asymmetry parameter ($\eta_A = 0.189$ and $\eta_Z = 0.136$) corresponds to the cold fission process (^{222}Ra $\rightarrow$ ^{132}Sn + ^{90}Sr).

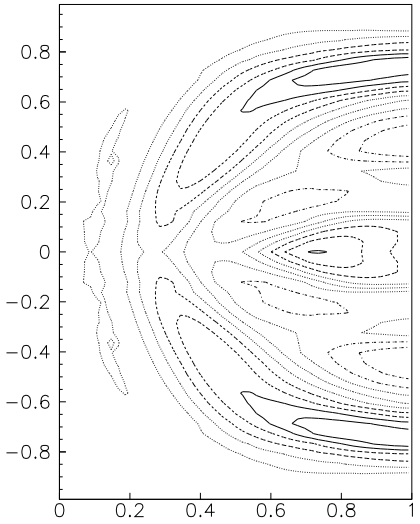

FIG. 8: Contour plot of shell and pairing corrections for ^{232}U vs $(R - R_i)/(R_t - R_i)$ and η.

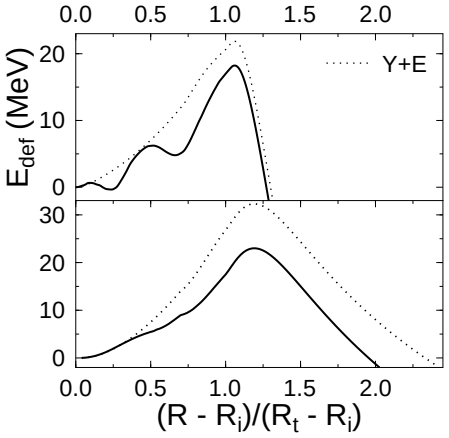

FIG. 9: A cut through the PES of ^{232}U at symmetry $\eta = 0$ (top) and for ^{24}Ne radioactivity with ^{208}Pb daughter (bottom).

^{232}U

Three PES versus the normalized separation distance and the mass asymmetry are plotted in Fig. 7: the macroscopic Y+EM deformation energy at the bottom; the microscopic shell plus pairing corrections at the center, and their sum (the total deformation energy) at the top. There are again three valleys on the shell plus pairing corrections and on the contour plot (Fig. 8) around $\eta \simeq 0.8$; 0.3, and 0.15. Unlike on the figure 2 for ^{222}Ra in which the valley due to Sn at a low mass asymmetry is not so deep, now this cold fission valley is well shaped and the trend continues for heavier nuclei such as ^{236}Pu and ^{242}Cm. An intermediate valley is produced by the magic neutron number $N_2 = 50$ of the light fragment. They are also present on the total PES at the top of Fig. 7. Here the deepest valley remains that of Sn, which is responsible for the cold fission; the ^{208}Pb + ^{24}Ne valley, explaining the ^{24}Ne radioactivity of ^{232}U, is laying on the Businaro-Gallone mountain, hence it is shallower.

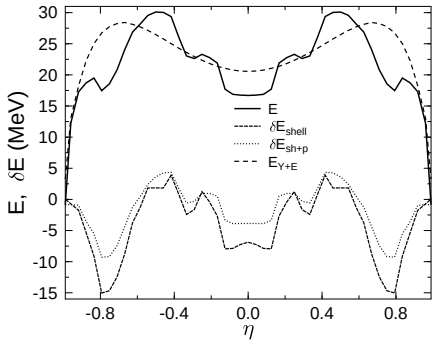

FIG. 10: Deformation energies at the touching point configurations ($R = R_t$) of ^{232}U vs the asymmetry η: E_{Y+EM} and E_{def} (top); shell + pairing corrections and only shell corrections (bottom).

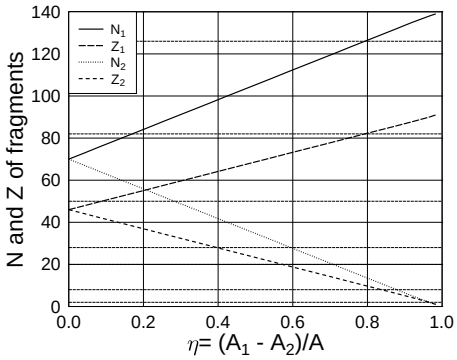

FIG. 11: Variation of the neutron and proton numbers of the two fragments with the mass asymmetry at the touching point, $R = R_t$ for ^{232}U.

In the upper part of Fig. 9 one can see a two humped barrier at $\eta = 0$. The example for ^{24}Ne emission from ^{232}U, shown at the bottom, provide justification for one of the basic assumption of the analytical superasymmetric fission model already mentioned in the previous subsection.

A cut of the PES at the touching point configura-

tion, $R = R_t$ is shown in Fig. 10 with the E_{Y+EM} (the smooth dashed line) and the total deformation energy E_{def} (heavy line) in the upper part. The three valleys mentioned above are present both on the total deformation energy (top) and in the lower part where the shell plus pairing correction (dotted curve) and only the shell corrections (dashed line) are plotted.

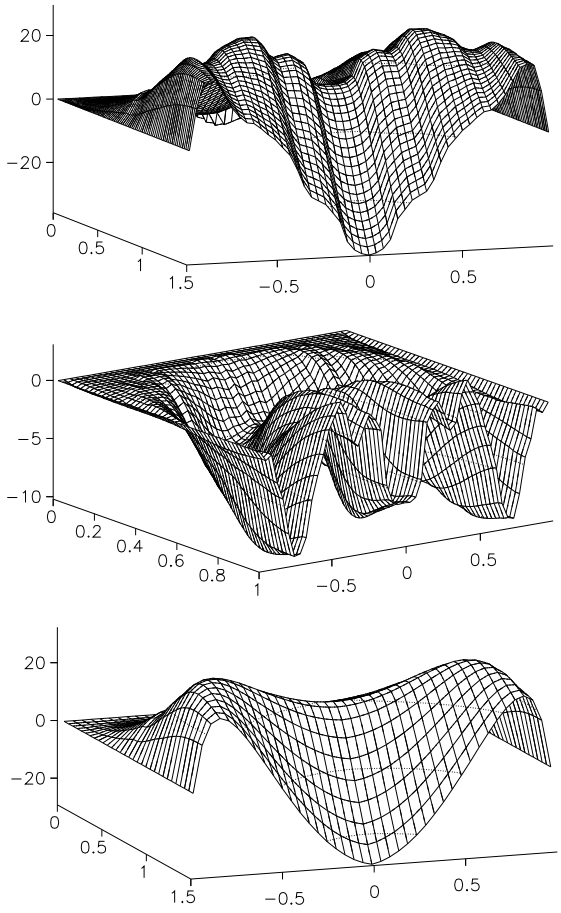

FIG. 12: PES of ^{236}Pu vs $(R - R_i)/(R_t - R_i)$ and $\eta = (A_1 - A_2)/(A_1 + A_2)$. Y+EM (bottom), Shell + Pairing corrections (center), and total deformation energy (top). The energies are expressed in MeV.

The figure 11 showing the variation of the neutron and proton numbers of the two fragments with the mass asymmetry at the touching point, $R = R_t$, for ^{232}U allows us to understand how the deep valleys from figure 10 are produced. The very deep valley around $\eta = 0.8$ ($\eta_A = 0.793$, $\eta_Z = 0.783$) is produced by the negative shell corrections due to two magic numbers $N_1 = 126$ and $Z_1 = 82$ (^{24}Ne radioactivity $^{232}\mathrm{U} \rightarrow {}^{208}\mathrm{Pb} + {}^{24}\mathrm{Ne}$). Another doubly magic heavy fragment, ^{132}Sn, produces the cold fission valley ($^{232}\mathrm{U} \rightarrow {}^{132}\mathrm{Sn} + {}^{100}\mathrm{Mo}$) at low mass and charge asymmetry ($\eta_A = 0.138$, $\eta_Z = 0.087$).

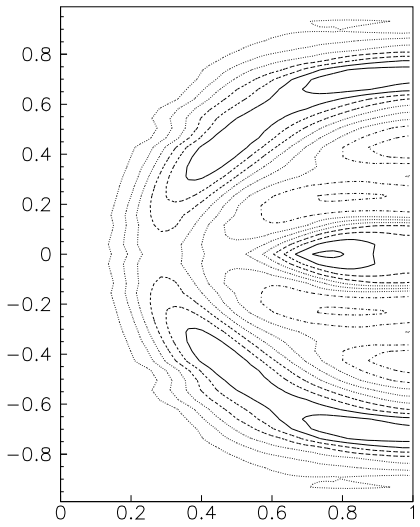

FIG. 13: Contour plot of shell and pairing corrections for ^{236}Pu vs $(R - R_i)/(R_t - R_i)$ and η.

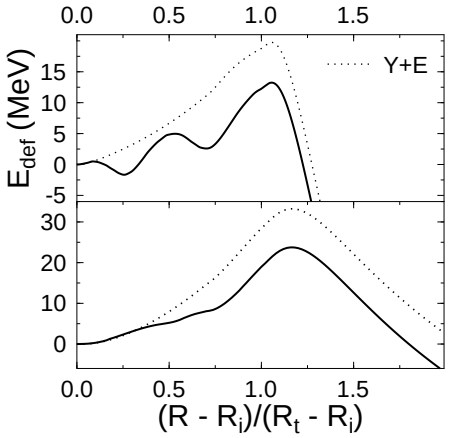

FIG. 14: A cut through the PES of ^{236}Pu at symmetry $\eta = 0$ (top) and for ^{28}Mg radioactivity with ^{208}Pb daughter (bottom).

The intermediate one ($\eta_A = 0.293$, $\eta_Z = 0.304$), quite shallow, is due to the neutron magic number of the light fragment $N_2 = 50$ ($^{232}\mathrm{U} \rightarrow {}^{150}\mathrm{Nd} + {}^{82}_{32}\mathrm{Ge}_{50}$).

^{236}Pu

PES versus the normalized separation distance and the mass asymmetry are plotted in Fig. 12, where Y+EM deformation energy is shown at the bottom, the shell plus pairing corrections at the center, and their sum (the total deformation energy) at the top. Very deep valleys

due to the doubly magic fragments ^{208}Pb and ^{132}Sn can be seen in the center of Fig. 12 and on the corresponding contour plot (Fig. 13) around $\eta \simeq 0.75$ and $\eta < 0.1$, respectively. At an intermediate value of the asymmetry parameter, $\eta \simeq 0.28$ there is another valley not so deep. These valleys may be also seen on the total PES at the top of Fig. 12. Here the deepest valley remains that of Sn, which is responsible for the cold fission; the ^{208}Pb + ^{28}Mg valley, explaining the ^{28}Mg radioactivity of ^{236}Pu, is laying on the Businaro-Gallone mountain, hence it is shallower.

Two plots obtained by cutting the PES at a given value of the asymmetry are shown in Fig. 14: a two humped barrier at $\eta = 0$ in the upper part and the barrier for ^{24}Ne spontaneous emission from ^{236}Pu, shown at the bottom. The last one provides a qualitative microscopic justification for the chosen barrier shape within the phenomenological ASAF.

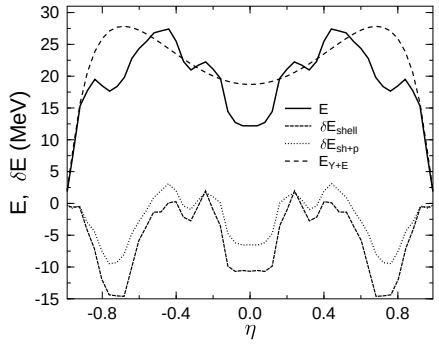

FIG. 15: Deformation energies at the touching point configurations ($R = R_t$) of ^{236}Pu vs the asymmetry η: E_{Y+EM} and E_{def} (top); shell + pairing corrections and only shell corrections (bottom).

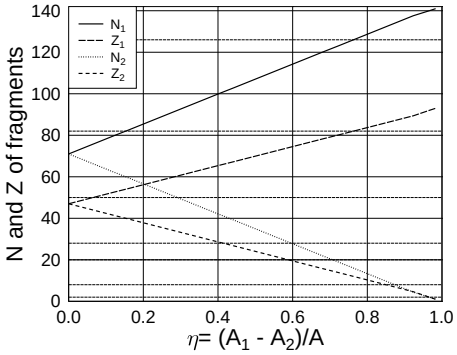

FIG. 16: Variation of the neutron and proton numbers of the two fragments with the mass asymmetry at the touching point, $R = R_t$ for ^{236}Pu.

One can see how deep are the three valleys by plotting in Fig. 15 a cut of the PES at the touching point configuration, $R = R_t$. In the upper part of this figure the macroscopic energy, E_{Y+E} (the smooth dashed line), and the total deformation energy, E_{def} (heavy line) can be seen. They exhibit few valleys of which that of Sn at lower values of η and that of Pb at higher η are the deepest ones. In the lower part of this figure there are two other curves representing the shell plus pairing correction (dotted curve), δE_{sh+p}, and only the shell corrections (dashed line), δE_{shell}. The valley at the intermediate value of the asymmetry parameter, $\eta \simeq 0.28$, is quite shallow.

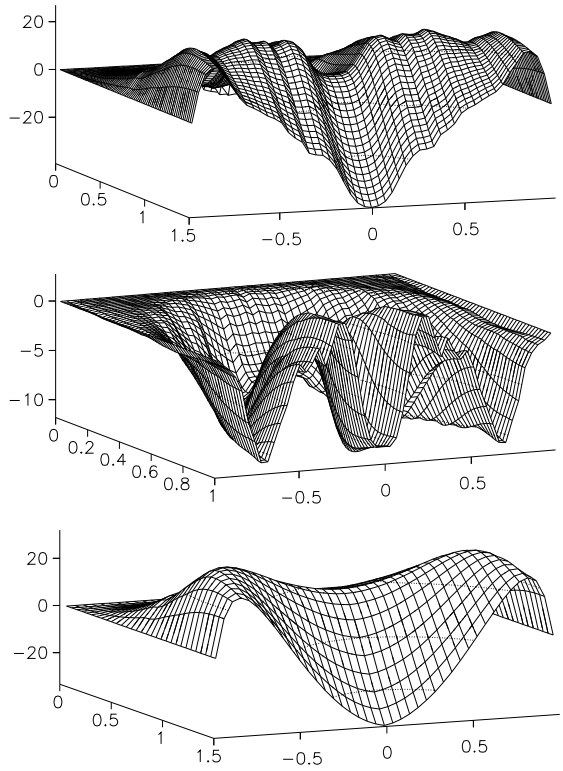

FIG. 17: PES of ^{242}Cm vs $(R - R_i)/(R_t - R_i)$ and $\eta = (A_1 - A_2)/(A_1 + A_2)$. Y+EM (bottom), Shell + Pairing corrections (center), and total deformation energy (top). The energies are expressed in MeV.

The variation of the neutron and proton numbers of the two fragments with the mass asymmetry at the touching point, $R = R_t$, for ^{236}Pu (figure 16) shows the occurence of magic numbers which generate the minima of the shell and pairing corrections producing the valleys on PES. The very deep valley around $\eta = 0.75$ ($\eta_A = 0.763$, $\eta_Z = 0.745$) is produced by reaching simultaneously two magic numbers $N_1 = 126$ and $Z_1 = 82$, ^{236}Pu $\rightarrow$ ^{208}Pb + ^{28}Mg. The cold fission valley (^{236}Pu $\rightarrow$ ^{132}Sn + ^{104}Ru) at a small asymmetry ($\eta_A = 0.119$, $\eta_Z = 0.064$) is the result of two magic numbers $Z_1 = 50$ and $N_1 = 82$. The intermediate valley ($\eta_A = 0.288$, $\eta_Z = 0.277$) is produced

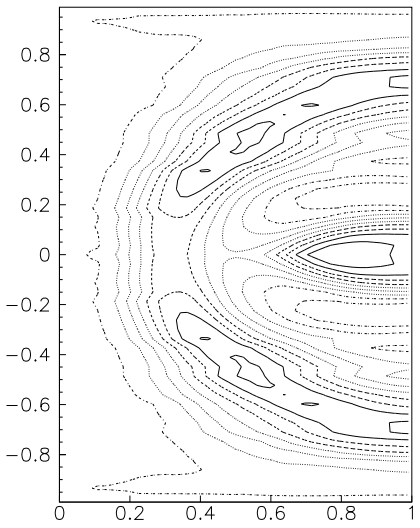

FIG. 18: Contour plot of shell and pairing corrections for ^{242}Cm vs $(R - R_i)/(R_t - R_i)$ and η.

by the magicity of the light fragment $N_2 = 50$, ^{236}Pu $\rightarrow$ ^{152}Nd + $^{84}_{34}$Se$_{50}$.

^{242}Cm

There are four valleys on the PES of figure 17 for ^{242}Cm at $\eta \simeq 0.7$; 0.4; 0.3, and 0.1. They are also present on the corresponding contour plot (Fig. 18). At the top of Fig. 17 the deepest valley remains that of cold fission due to a doubly magic heavy fragment ^{132}Sn, and the

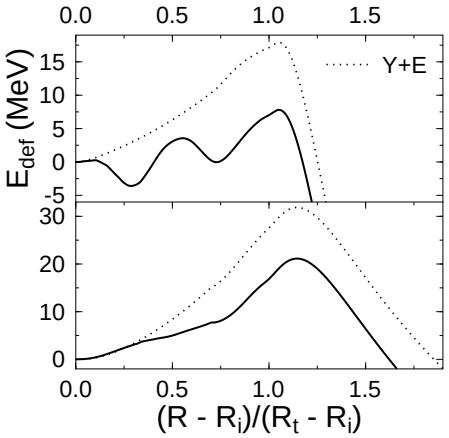

FIG. 19: A cut through the PES of ^{242}Cm at symmetry $\eta = 0$ (top) and for ^{34}Si radioactivity with ^{208}Pb daughter (bottom).

silicon-and-lead valley the ^{208}Pb + ^{34}Si, explaining the ^{34}Si radioactivity of ^{242}Cm.

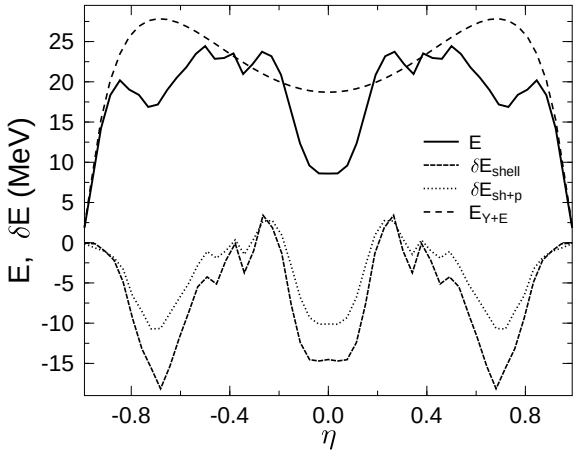

FIG. 20: Deformation energies at the touching point configurations ($R = R_t$) of ^{242}Cm vs the asymmetry η: E_{Y+EM} and E_{def} (top); shell + pairing corrections and only shell corrections (bottom).

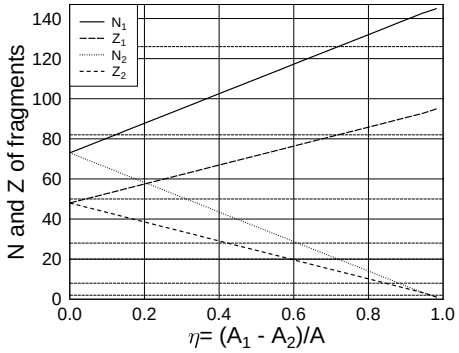

FIG. 21: Variation of the neutron and proton numbers of the two fragments with the mass asymmetry at the touching point, $R = R_t$ for ^{242}Cm. Every time a nucleon number reaches a magic value, the corresponding shell correction has a local minimum. The very deep valley around $\eta = 0.719$ is produced by reaching simultaneously three magic numbers $N_1 = 126$, $N_2 = 20$, and $Z_1 = 82$.

Two plots obtained by cutting the PES at a given value of the asymmetry are shown in Fig. 19. In the upper part one can see the two humped barrier and at the bottom the barrier for ^{34}Si emission from ^{242}Cm. Having a smaller height and width compared to the (dotted line) macroscopic Y+EM barrier, it is very similar to the barrier used in ASAF which was lower and narrower than the the Myers-Swiatecki's LDM barrier.

One can see how deep are the four valleys on the PES by plotting in Fig. 20 a cut of the PES at the touching point configuration, $R = R_t$. In the upper part of this figure the macroscopic energy, E_{Y+E}, (the smooth dashed line) and the total deformation energy, E, (heavy line) can be seen. In the lower part there are two other curves representing the shell plus pairing correction (dot-

ted curve), δE_{sh+p}, and only the shell corrections (dashed line), δE_{shell}.

The figure 21 shows the variation of the neutron and proton numbers of the two fragments with the mass asymmetry at the touching point, $R = R_t$, for ^{242}Cm. Like in the preceding subsections, the deepest valley on the shell and pairing corrections is produced by the very strong shell effect of the heavy fragment ^{208}Pb (^{242}Cm $\rightarrow$ ^{208}Pb + $^{34}_{14}$Si$_{20}$) at $\eta_A = 0.719$ and $\eta_Z = 0.708$; here there is also a contribution coming from the neutron number of the light fragment, $N_2 = 20$. The deepest valley on the total deformation energy is the cold fission one at $\eta_A = 0.091$, $\eta_Z = 0.042$, where ^{242}Cm $\rightarrow$ ^{132}Sn + ^{110}Pd. The two intermediate valleys are produced mainly by $N_2 = 50$ and $Z_2 = 28$. One has at $\eta_A = 0.306$, $\eta_Z = 0.292$ the decay ^{242}Cm $\rightarrow$ ^{158}Sm + $^{84}_{34}$Se$_{50}$ and at $\eta_A = 0.421$, $\eta_Z = 0.417$ ^{242}Cm $\rightarrow$ ^{172}Er + $^{70}_{28}$Ni$_{42}$.

In conclusion the strong shell effect associated to the doubly magic character of the daughter ^{208}Pb, observed in the systematic analysis of experimental results [1], comes from a valley present on the potential energy surfaces of cluster emitters at a relatively high value of the asymmetry parameter $\eta \simeq 0.7 - 0.8$. Despite its high depth on the microscopic corrections PES, on the total deformation energy it appears shallower since it is added to the Businaro-Gallone mountain of the Y+EM macroscopic energy. The potential barrier shape of heavy ion radioactivity obtained from the first time by using the macroscopic-microscopic method provides further support for the particular choice of the barrier within the analytical superasymmetric model. The depth of the cold fission valley produced by the doubly magic heavy fragment ^{132}Sn, which is small for ^{222}Ra, increases with the mass number of the parent nucleus being comparable to the lead valley on the microscopic corrections PES of ^{242}Cm. Some other intermediate shallower valleys are produced by the magicity of the light fragment: $Z_2 = 28$ for ^{222}Ra parent; $N_2 = 50$ for ^{232}U parent; $N_2 = 50$ for ^{236}Pu; $N_2 = 50$ and $Z_2 = 28$ for ^{242}Cm.

This work was partly supported by Deutsche Forschungsgemeinschaft, Bonn, and by Ministry of Education and Research, Bucharest. We acknowledge also the support by Prof. S. Hofmann Gesellschaft für Schwerionenforschung (GSI), Darmstadt.

* poenaru@th.physik.uni-frankfurt.de

[1] D.N. Poenaru, Y. Nagame, R.A. Gherghescu, W. Greiner, *Phys. Rev.*, **C65** (2002) 054308; Erratum **C66** 049902.
[2] D.N. Poenaru, W. Greiner, in *Nuclear Decay Modes*, (IOP Publishing, Bristol, 1996), Chap. 6, pp. 275.
[3] D. N. Poenaru, D. Schnabel, W. Greiner, D. Mazilu, R. Gherghescu, *Atomic Data Nucl. Data Tables*, **48** (1991) 231.
[4] R. A. Gherghescu, *Phys. Rev.* **67** (2003) 014309.
[5] V. M. Strutinsky, *Nucl. Phys.* **A 95** (1967) 420.
[6] W. Scheid, W. Greiner, *Z. Phys.* **A 226** (1969) 364.
[7] H. J. Krappe, J. R. Nix, A. J. Sierk, *Phys. Rev.* **C 20** (1979) 992.
[8] D. N. Poenaru, M. Ivaşcu, D. Mazilu, *Comput. Phys. Comm.* **19** (1980) 205.
[9] P. Möller, J. R. Nix, W. D. Myers, and W. J. Swiatecki, *Atomic Data Nucl. Data Tables* **59** (1995) 185.
[10] M. Bolsterli, E. Fiset, J. R. Nix, J. Norton, *Phys. Rev* **C 5** (1972) 1050.
[11] W. D. Myers, W. J. Swiatecki, *Nucl. Phys.* **A 81** (1966) 1.